Rain Induced Co-channel Interference at 60 GHz and 300 GHz Frequencies

Harri Juttula*, Joonas Kokkoniemi†, Janne Lehtomäki†, Anssi Mäkynen‡, and Markku Juntti†
*Unit of Measurement Technology, University of Oulu, P.O.BOX 127, 87400 Kajaani, Finland
Email: harri.juttula@oulu.fi
†Centre for Wireless Communications (CWC), University of Oulu, P.O. Box 4500, 90014 Oulu, Finland
Email: joonas.kokkoniemi@oulu.fi, janne.lehtomaki@oulu.fi, markku.juntti@oulu.fi
‡Optoelectronics and Measurement Techniques Unit, University of Oulu, P.O.Box 4500, 90014 Oulu, Finland
Email: anssi.makynen@oulu.fi

***Abstract*—Results at mm wave frequencies have shown that it is important to evaluate co-channel interference between directional beams that cross each other. Terahertz frequency bands, especially around 300 GHz, has been considered for future wireless communications. As far as we know, no work has considered the rain induced interference at THz frequencies. In this work, we evaluate the rain induced interference at 300 GHz. Results are calculated also at 60 GHz in order to make a comparison. We combined bistatic radar equation, first order multiple scattering approximation and full Mie scattering calculations to existing drop size distribution models to estimate interference due to rain. Considered effective path lengths between transmitter and receiver are 100 m and 500 m and the effect of selected drop size distribution is studied. Overall interference levels was observed to be approximately 20 dBm smaller at 300 GHz than at 60 GHz and angular dependency of interfering power was much more forward oriented for 300 GHz frequency. The results show that rain induces interference has significantly different behaviour at THz as compared to lower frequencies.**

I. Introduction

Millimeter-wave (mmWave, 30-300 GHz) and terahertz communication (0.3-10 THz) systems are expected to revolutionize short range communications in the near future [1]. These high frequency bands offer superior bandwidths to those of the lower (below 6 GHz) frequency bands. This allows the next big leap in the achievable data rates. Whereas the large path loss in the channel limits the operational range, high gain antennas can enable the utilization of the higher frequencies also in short range backhauling ($\sim$100 meters). In such mostly outdoor applications, the free space loss or molecular absorption loss [2] are not the only significant loss mechanisms. Possible rain and fog losses add to the total link budget.

In terahertz range extinction of electromagnetic wave due to hydrometeors and molecular absorption in atmospheric gases are major attenuating factors. Extinction due to rain can be further divided into absorption by water and scattering by water droplets. It is due to the scattered component of the electromagnetic wave that part of the transmitter power may be experienced as interference between nearby links. In this section interference is estimated theoretically for 300 GHz frequency with 100 m and 500 m effective path lengths with varying transmitter and receiver orientations and rain rates up to 20 mm/h. Results are also compared with 60 GHz frequency for 100 m effective path length. Calculations are based on bistatic radar equation, the Mie scattering theory and first order multiple scattering approximation.

Mie scattering theory is well established method to model scattering and absorption by spherical particles. In millimeter and terahertz wavelengths, for example, the Mie theory has been used to explain experimental results for spesific attenuation due to water droplets or dust particles for direct links in laboratory controlled environments [3]–[5]. Specific attenuation given by the Mie theory has been shown to match experiments in artificial rain for up to 500 mm/h rain rates which is well above normal atmospheric rain conditions.

The rest of this paper is organized as follows. Section 2 introduces the theoretical models utilized in this work: bistatic radar equation, the Mie scattering theory and rain drop size distribution models. Section 3 gives the numerical results for specific attenuation and co-channel interference and Section 4 concludes the paper.

II. Theory

A. Bistatic Coupling

Rain induced interference can be thought as scattered power in the overlapping volume of transmitter and nearby receiver. In the first order multiple scattering approximation, only scattering in the common volume is assumed to reach the receiver, while scattering along the path from transmitter to beam intersection and to receiver is treated as lost power that is included in extinction along with absorption. This assumption has been experimentally verified at 94 GHz [6].

The ratio of the received and transmitted power due to rain scattering can be calculated with a well-known bistatic radar equation. We have used formulation given by [7]:

$$\frac{P_r}{P_t} = \frac{\lambda^2}{4\pi^3} \int_V \frac{G_t G_r}{(r_t r_r)^2} \eta(\theta_s) A_{air} A_{rain} dV \qquad (1)$$

This project (TERRANOVA) was supported by Horizon 2020, European Unions Framework Programme for Research and Innovation, under grant agreement no. 761794. This work was also supported in part by Academy of Finland 6Genesis Flagship under grant no. 318927.

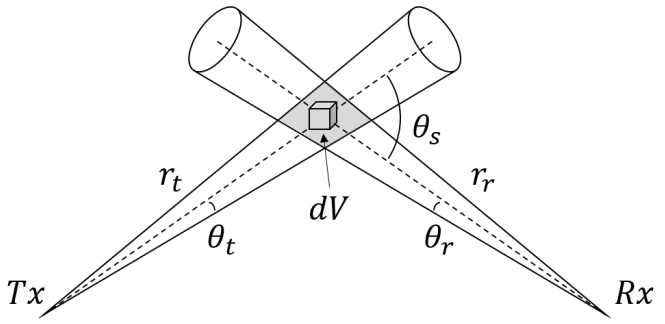

Fig. 1. Bistatic coupling geometry for overlapping transmitter (Tx) and receiver (Rx) beams with common volume. Distances r_t and r_r are measured from the volume element dV.

where λ is wavelength, G_t and G_r are directional gain functions for transmitter and receiver antennas, r_t and r_r are transmitter and receiver distances to scattering volume element dV, $\eta(\theta_s)$ is the bistatic scattering cross section, A_{air} and A_{rain} are path attenuations due to atmospheric absorption and rain induced scattering. For first order multiple scattering approach rain induced path attenuation can be written as $A_{rain}(r) = \exp(-\mu_{ext} r)$ where μ_{ext} is extinction coefficient that includes both absorption and scattering and can be calculated with the Mie scattering theory if the drop size distribution and complex refractive index of water are known. Volume integral in (1) is performed over the common volume of overlapping beams. Geometry of the situation is illustrated in Fig. 1. It should be noted that attenuation A_{rain} in equation (1) is considered for the whole traveled path from Tx to Rx not only in common volume of beams.

Bistatic scattering cross section η in the bistatic radar equation (1) depends on the scattering properties of rain drops and their size distribution and can be calculated by integrating over all drop sizes

$$\eta(\theta_s) = \int_0^\infty N(D)\sigma_{sca}(D)P(D,\theta_s)dD \tag{2}$$

where D is drop diameter, θ_s is scattering angle measured from original direction, $N(D)$ is rain drop size distribution (DSD), σ_{sca} is scattering cross section and $P(D,\theta_s)$ is scattering phase function which describes the probability distribution of the scattered wave direction. Cross section and phase function can be obtained from scattering theories and DSD is usually a function that is fitted to real measured DSD data.

B. Mie Scattering Theory

At 300 GHz frequency the wavelength of the EM wave and typical diameters of raindrops are close to each other. This leads to a diameter to wavelength ratio that is in the Mie scattering regime. The Mie scattering can be used to calculate scattering properties of any spherical particle with known complex refractive index. For very small particles when $D \ll \lambda$ solution given by the Mie theory approaches the Rayleigh approximation. The Mie scattering theory can be therefore used to treat rain as an ensemble of particles whose diameters are both in the Mie and Rayleigh regimes. Theoretical treatment used in this work is based on the formulation presented in book by Bohren and Huffman [8].

If we assume the rain drops to be homogeneous spherical particles with known radii and refractive index we can use the Mie scattering theory to get an exact solution for scattering properties of an individual sphere. Extinction, scattering and absorption cross sections can be written as:

$$\sigma_{ext} = \frac{\pi D^2}{x^2}\sum_{n=1}^{\infty}(2n+1)\Re(a_n + b_n) \tag{3}$$

$$\sigma_{sca} = \frac{\pi D^2}{x^2}\sum_{n=1}^{\infty}(2n+1)(|a_n|^2 + |b_n|^2) \tag{4}$$

$$\sigma_{abs} = \sigma_{ext} - \sigma_{sca} \tag{5}$$

Mie scattering coefficients a_n and b_n are complex functions of drop diameter, refractive index and wavelength of EM wave. Size parameter x defined as $x = 2\pi D/\lambda$. Extinction cross section can be related to the geometrical cross section particles by defining extinction efficiency $\sigma_{ext} = \pi D^2 Q_{ext}$. Scattering and absorption efficiencies can be defined similarly. Angular dependency of the Mie scattering can be described with scattering phase function. For unpolarized incident wave phase function is:

$$P(\theta) = \frac{|S_1(\theta)|^2 + |S_2(\theta)|^2}{\pi x^2 Q_{sca}} \tag{6}$$

where $S_i(\theta)$ terms are elements of scattering amplitude matrix given by the Mie theory. Phase function is usually normalized so that integration over all angles result to unity.

C. Rain Drop Size Distribution

Drop size distributions are typically functions that give number of particles in volume unit as a function of rain rate. One commonly used DSD is Marshall-Palmer drop size distribution [9]. Marshall-Palmer distribution is exponential function that reaches maximum at 0 mm diameter. The distribution overestimates the number of small droplets and it is valid for drops with diameter greater than 1.5 mm. In the traditional radio and communication frequencies, this has not been a problem since the scattering efficiency of very small particles is insignificant. In terahertz frequencies one cannot ignore small drop sizes. In reality the drop size distributions resemble more log-normal or gamma distribution than the exponential function. For this reason, we chose to use a distribution that has a clear maximum and avoids overestimating number of small drops. DSD we used in this work is one given by [10]:

$$N(D) = 1.98 \times 10^4 R^{-0.384} D^{2.93} \exp(-5.38 R^{-0.186} D) \tag{7}$$

where R is rain rate in mm/h and D is drop diameter in mm. Equation (7) has unit $\mathrm{m}^{-3}\mathrm{mm}^{-1}$ and it describes the number of drops with diameter between D and $D + dD$ in one cubic meter of air. Fig. 2 shows DSD (7) at four different rain rates used in this work together with the corresponding Marshall-Palmer distributions.

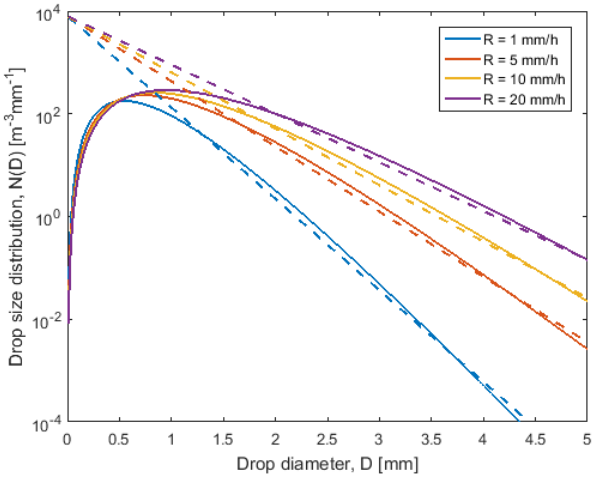

Fig. 2. Comparison drop size distributions at rain rates used in this paper. Solid lines are de Wolf's and dashed lines are corresponding Marshall-Palmer drop size distributions.

III. Results

Solving the volume integral (1) requires full Mie solution for a wide range of drop sizes. In order to minimize the complex cross section calculations we chose a lookup table approach and pre-calculated Mie solutions for spheres between 0.1 μm to 10 mm with 0.1 μm step interval for 60 and 300 GHz. Complex refractive index of water at these frequencies were taken from [11]. The actual calculations were performed with a Matlab implementation of the Mie equations by [12], [13] and they provided us with extinction and scattering cross sections and scattering phase functions for each drop size. Few examples of scattering phase functions are shown in Fig. 3 for both frequencies. It can be seen from the figures that at 60 GHz frequencies Mie solutions resemble more Rayleigh type scattering while at 300 GHz scattering has more complex angular dependency and is much more forward oriented when diameter is greater than 1 mm. Even at d = 1 mm 300 GHz has forward oriented scattering pattern whereas 60 GHz the pattern is almost flat. This behavior is as expected as the size parameter x of drops are larger at 300 GHz frequency. We checked the functionality of the Mie code against online Mie calculator [14] and by replicating results in paper [15].

After verifying the Mie code we calculated specific attenuation due to rain. For this we solved extinction coefficient of rain for both Marshall-Palmer and de Wolf's distributions for several rain rates and calculated the attenuation with Beer-Lambert attenuation law $I(r) = I_0(r)\exp(-\mu_{ext}r)$. Attenuations are shown in Fig. 4 in dB/km together with specific attenuation given by ITU-838 model [16]. At 60 GHz frequency de Wolf's distribution leads to slightly lower and Marshall-Palmer to slightly higher specific attenuation than ITU model. At 300 GHz differences become more prominent. This means although ITU model gives relatively good average results, at 300 GHz, the actual attenuation (depending on the actual DSD) can differ up to around 5 dB per km. For link

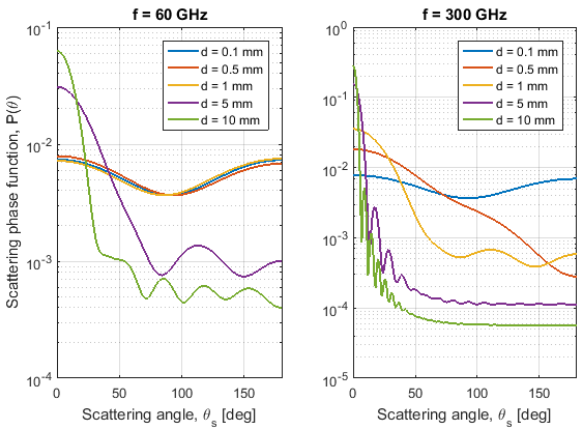

Fig. 3. Examples of normalized scattering phase function $P(\theta)$ for few drop diameters at 60 GHz and 300 GHz frequencies. Higher frequency leads to more forward oriented scattering for similar drop sizes.

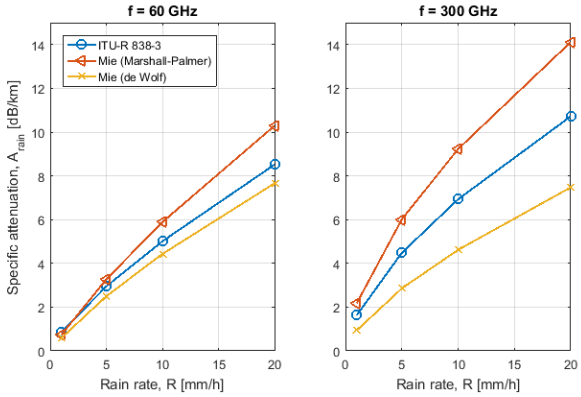

Fig. 4. Specific attenuations at 60 GHz (left) and 300 GHz (right). Specific attenuation becomes more sensitive to the DSD model with increasing frequency.

design, this indicates the need to for additional margins when using the ITU model. This is in line of observations that while attenuation due to rain becomes nearly independent of frequency above 100 GHz, it becomes very sensitive to the drop size distribution of rain [17], [18].

The number of geometries that can describe interference via bistatic coupling is infinite as positions and directions of Tx and Rx can be chosen arbitrarily. In our calculations we chose to use 100 m and 500 m effective Tx to Rx distance. We define the effective distance to be measured as total distance from Tx to point P and from P to Rx. Point P is the intersection of line-of-sight directions of Tx and Rx pair and θ_s defines the angle between their directions as shown in Fig. 1. Both Tx and Rx were set to be equidistant from P so that in first case distances r_t and r_r are 50 m and in the second case 250 m. Angle θ_s was varied between 10 to 170 degrees. Smaller and larger angles were omitted due to possible singularities in numerical integrals. Half angles θ_t and θ_r of constant gain transmitter and receiver cones were 2 degrees and 0.5 degrees for 100 m and 500 m effective distances respectively. Antenna gains for these

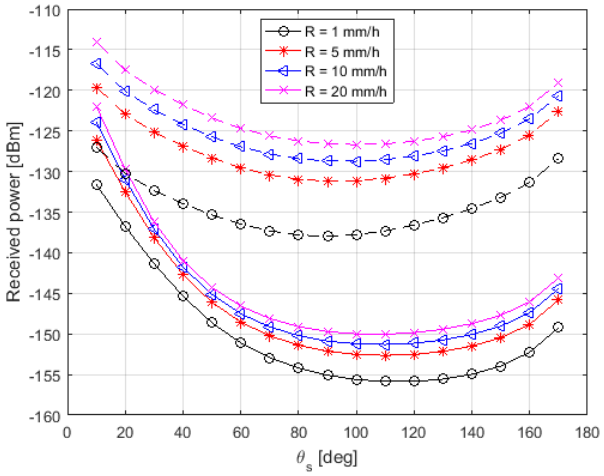

Fig. 5. Received power for 1 mW transmitter for 100 m effective path length at 60 GHz (dashed lines) and 300 GHz (solid lines) frequencies at rain rates from 1 mm/h to 20 mm/h.

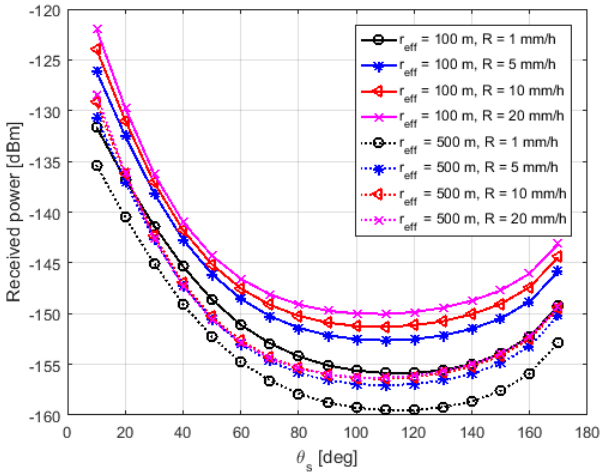

Fig. 6. Received power for 1 mW transmitter for 100 m and 500 m effective path lengths at 300 GHz with different rain rates.

cones were estimated with equation $G = -10\log_{10}(0.5(1 - \cos\theta))$ to be +35.2 dB and +47.2 dB respectively.

Received power for 100 m effective path lengths are shown in Fig. 5 for both 60 GHz and 300 GHz for rain rates between 1 mm/h to 20 mm/h. These values include antenna gains and path attenuation due to atmospheric absorption according to ITU-676 model [19]. 60 GHz frequency shows higher overall interference with minimum at approximately 90 degree beam angle. Increased coupling at small and large angles is due to increase in common volume since the scattering has strong Rayleigh like behavior at 60 GHz. In 300 GHz case interference is much higher at small beam angles. This is due to stronger forward oriented scattering due to different wavelength. While the overall level of received power was much lower for 300 GHz it may surpass 60 GHz at small angles. In reality interference at small angles may be further increased for 300 GHz since the first order multiple scattering approximation may break if scattering component of extinction is not lost from beam due to its forward oriented nature. In Fig. 6 received interference is shown for both 100 m and 500 m effective path lengths at 300 GHz frequency.

We also compared the effect of drop size distribution for 100 m effective path length case. Previous results that were based on de Wolf's DSD model are compared in Fig. 7 with similar calculations with Marshall-Palmer DSD. There is slight increase in interference with Marshall-Palmer DSD for larger rain rates at 60 GHz but the difference is not large. Situation changes for 300 GHz frequency in which the Marshall-Palmer DSD leads to approximately 5 dB larger overall interference.

Overall, theoretical co-channel interference response is not very large unlike it has previously been shown [20]. However, it may become an issue in certain cases, such as co-channel interference between high-powered devices and low powered sensor applications.

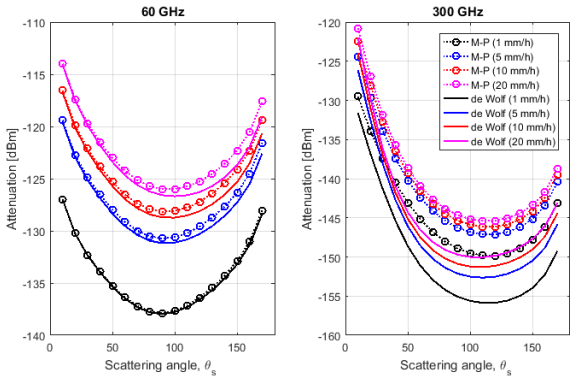

Fig. 7. Effect of drop size distribution model on received power at different transmitter and receiver orientation angles. Solid lines are calculated using de Wolf DSD and dashed lines with Marshall-Palmer DSD.

IV. Conclusions

Interference due to rain induced scattering was estimated with the bistatic radar equation, the first order multiple scattering assumption and the Mie scattering theory at 60 GHz and 300 GHz frequencies. Up to 20 mm/h rain rates were considered and two different rain drop size distributions were used to model rain. Interference was calculated for 100 m and 500 m effective path lengths with varying transmitter and receiver orientations.

Calculations indicate that the overall interference level is smaller at 300 GHz than at 60 GHz frequency with the exception of cases when receiver is very close to the line of sight direction of transmitter which is due to the much more forward oriented nature of scattering at higher frequencies. Calculations also show that the underlying rain drop size distribution becomes important factor for interference at 300 GHz and may indicate a need for additional margins when using the ITU model. The popular Marshall-Palmer distribution should not be used when smaller than 1 mm diameter drops are

expected to have significant role in extinction and scattering characteristics of rain.

REFERENCES

[1] I. F. Akyildiz, J. M. Jornet, and C. Han, "Terahertz band: Next frontier for wireless communications," *Phys. Commun.*, vol. 12, pp. 16–32, Sep. 2014.

[2] J. M. Jornet and I. F. Akyildiz, "Channel modeling and capacity analysis for electromagentic nanonetworks in the terahertz band," *IEEE Trans. Wireless Commun.*, vol. 10, no. 10, pp. 3211–3221, Oct. 2011.

[3] K. Su, L. Moeller, R. B. Barat, J. F. Federici, "Experimental comparison of terahertz and infrared data signal attenuation in dust clouds," *J. Opt. Soc. Am. A*, vol. 29, no. 11, 2012.

[4] J. Ma, F. Vorrius, L. Lamb, L. Moeller, J. F. Federici, "Experimental comparison of terahertz and infrared signaling in laboratory-controlled rain," *J. Infrared Millim. Terahertz Waves*, vol. 36, no. 9, pp. 856–865, 2015.

[5] J. Ma, F. Vorrius, L. Lamb, L. Moeller, J. F. Federici, "Comparison of experimental and theoretical determined terahertz attenuation in controlled rain," *J. Infrared Millim. Terahertz Waves*, vol. 36, no. 12, pp. 1195–1202, 2015.

[6] C. Gloaguen, J. Lavergnat, "94 GHz bistatic scattering in rain," IEEE Trans. Antennas Propagation, vol. 44, pp. 1247-1258, 1996.

[7] C. Capsoni, L. Luini, M. DAmico, "The MultiEXCELL model for the prediction of the radio interference due to hydrometeor scattering," in Proc. 4th Europ. Conf. Antennas Propag., Barcelona, Spain, 2010.

[8] C. F. Bohren, D. R. Huffman, "Absorption and scattering of light by small particles," Wiley, New York, 1983.

[9] J. S. Marshall, W. M. K. Palmer, "The distribution of raindrops with size," Journal of Meteorology, vol. 5, no. 4, pp.165–166, 1948.

[10] D. A. de Wolf, "On the Laws-Parsons distribution of raindrop sizes," Radio Science, vol. 36, no. 4, pp. 639-642, 2001.

[11] D. J. Segelstein, The complex refractive index of water, MSc Thesis, University of Missouri, Kansas City, USA, 1981.

[12] J. Schäfer, Implementierung und Anwendung analytischer und numerischer Verfahren zur Lösung der Maxwellgleichungen für die Untersuchung der Lichtausbreitung in biologischem Gewebe, PhD thesis, Univerität Ulm, 2011.

[13] J. Schäfer, S.-C. Lee, A. Kienle, Calculation of the near fields for the scattering of electromagnetic waves by multiple infinite cylinders at perpendicular incidence, J. Quant. Spectrosc. Radiat. Trans. vol. 113, no. 16, pp. 2113–2123, 2012.

[14] S. Prahl, "Mie scattering calculator", 2018, [online] Available: https://omlc.org/calc/mie_calc.html

[15] T. A. Bashkatova, A. N. Bashkatov, V. I. Kochubey, V. V. Tuchin , "Light-scattering properties for spherical and cylindrical particles: a simple approximation derived from Mie calculations", Proc. SPIE, vol. 4241, 2001.

[16] "Specific attenuation model for rain for use in prediction methods", ITU-R, Recommendation P.838-3, 2005.

[17] S. Das, A. Maitra, A. K. Shukla, "Rain attenuation modeling in the 10-100 GHz frequency using drop size distributions for different climatic zones in tropical India," Prog. Electromagn. Res. B, vol. 25, pp. 211-224, 2010.

[18] S. Ishii, S. Sayama, T. Kamei, "Measurement of Rain Attenuation in Terahertz Wave Range," Wireless Engineering and Technology, vol. 2, pp. 119-124, 2011.

[19] "Attenuation by atmospheric gases", ITU-R, Recommendation P.676–10, 2013.

[20] H. T. van der Zanden, R. J. Watson, M. H. A. J. Herben, "Rain-induced bistatic scattering at 60 GHz," EURASIP J. Wirel. Commun. Netw., vol. 2007, 2007.